Modeling of the Centerless Infeed (Plunge) Grinding Process

Kang Kim*

School of Mechanical and Automotive Engineering, Kookmin University, 861-1 Jungreung-dong, Sungbook-gu, Seoul 136-702, Korea

A computer simulation method for investigating the form generation mechanism in the centerless infeed (plunge) grinding process is described. For a 3-D simulation model of form generation, contact points are assumed to be on least squares contact lines at the grinding wheel, regulating wheel, and work-rest blade. Using force and deflection analyses, the validity of this assumption is shown. Based on the 2-D simulation model developed in the previous work and the least squares contact line assumption, a 3-D model is presented. To validate this model, simulation results were compared with the experimental works. The experiments and computer simulations were carried out using three types of cylindrical workpiece shapes with varying flat length. The experimental results agree well with the simulation. It can be seen that the effect of flat end propagated to the opposite end through workpiece reorientation.

Key Words: Centerless Infeed (Plunge) Grinding, Least Squares Contact Line (LSCL), Workpiece Reorientation

1. Introduction

In spite of the development of new precision manufacturing processes, centerless grinding process still remains the most accurate and popular process for machining cylindrical parts. Conventionally, the most widely known control parameter for cylindrically ground parts has been the roundness. With the growing requirement for accuracy in a cylindrical feature, straightness and parallelism also become major tolerances affecting the quality of ground parts. For example, a survey carried out in this work of a diesel engine fuel injector factory revealed that over 80% of plungers did not satisfy the specified cylindricity tolerance and the resultant clearance. The average ratio of out-of-roundness, straightness, and taper was found to be 2 : 1 : 2.

* **E-mail** : kangkim@kookmin.ac.kr
TEL : +82-2-910-4676; **FAX** : +82-2-910-4839
School of Mechanical and Automotive Engineering, Kookmin University, 861-1 Jungreung-dong, Sungbook-gu, Seoul 136-702, Korea. (Manuscript **Received** February 3, 2003; **Revised** April 14, 2003)

The representative theoretical researches about rounding mechanisms in centerless grinding were presented by Dall (1946), Yonetsu (1959), and Rowe and Barash (1964). Their researches were based on the infeed grinding process, and were limited to 2-D modeling to investigate the influences of centerless grinding variables on the out-of-roundness of the ground part. In the 2-D case, the governing equation was developed under the assumption that the shape of any cross-sectional layer is exactly the same. The objective of this research is to develop a 3-D computer simulation method for a cylindrical form generation mechanism in a centerless infeed grinding process. The fundamental form of the 3-D model is the same as that of the 2-D model developed in the previous work (Kim et al., 1992a). However, it is essential to consider all contact points at the grinding wheel, regulating wheel, and work-rest blade. To overcome this difficulty, an averaging concept defining contact lines between the workpiece and the machine elements is required to incorporate the effects of contact points which are not in the same layer. In this paper, a straight line fitted by least squares is selected as the contact

line because of mathematical simplicity. The interference phenomena (Kim et al., 1992b) are also included to formulate the least squares contact lines (LSCL). To check the feasibility of contact line modeling, force and deflection at a contact point are also analyzed. The basic concepts of the apparent depth of cut, the interference restrictions, and the machining elasticity concept in Kim, Chu, and Barash's researches (1992a, 1992b) are adopted in this work.

2. Force and Deflection Analyses

Figure 1 shows the simplified 2-D configuration of the centerless grinding geometry where θ is the angle of rotation ($\angle O_gOX$) between the initial reference line OX on the workpiece and the grinding wheel contact normal shown as OO_g, α is the angle ($\angle O_gOB$) between the line OO_g and the normal line OB of the work-rest blade surface, β is the supplementary angle ($\pi-\angle O_gOO_r$) between the line OO_r connecting the work-piece center and the regulating wheel center and the line OO_g, and γ is the top angle of the work-rest blade. The reference line OX coincides with the line OO_g at the beginning of grinding.

Figure 2 shows a two-dimensional free body diagram of a workpiece during a centerless grinding process, where F_n is a normal force at the grinding wheel contact point, F_t is a tangential force at the grinding wheel contact point, B_n is a normal force at the work-rest blade contact point, B_t is a tangential force at the work-rest blade contact point, R_n is a normal force at the regulating wheel contact point, R_t is a tangential force at the regulating wheel contact point, G_w is a weight of the workpiece δ is the angle between the grinding wheel contact normal and the line connecting the grinding wheel center and the regulating wheel center, and τ is the angle between the regulating wheel contact normal and the line connecting the grinding wheel center and the regulating wheel center.

Force equilibrium conditions can be expressed as follows:

$$F_t-B_t-R_t=0 \tag{1}$$

$$F_n\cos\delta+F_t\sin\delta+B_n\cos\gamma-B_t\sin\gamma-R_n\cos\tau-R_t\sin\tau=0 \tag{2}$$

$$F_n\sin\delta-F_t\cos\delta+B_n\sin\gamma+B_t\cos\gamma+R_n\sin\tau-R_t\cos\tau-G_w=0 \tag{3}$$

While the workpiece rotates, there is a slip between the work-rest blade and the workpiece. B_t is kinetic frictional force at the work-rest blade contact point given by:

$$B_t=\mu_kB_n \tag{4}$$

where μ_k is the kinetic friction coefficient.

In centerless grinding process, the regulating wheel drives the workpiece and provides a braking action (ASM International, 1989). Thus R_t is less than or equal to the static friction force between the regulating wheel and the workpiece. Then the relation between R_t and R_n is given as:

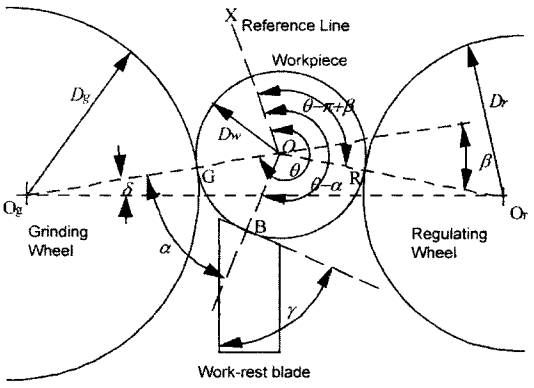

Fig. 1 Centerless grinding geometry

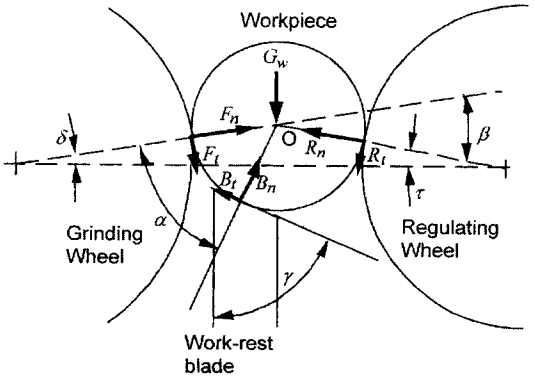

Fig. 2 Two-dimensional free body diagram of workpiece

$$R_t = \kappa R_n \leq \mu_r R_n \tag{5}$$

where μ_r is static friction coefficient and κ is a constant which is less than or equal to the static friction coefficient at the regulating wheel contact point.

Figure 2 shows the relationships among the angles, α, β, δ, τ, and γ, where

$$\alpha = \gamma - \delta \tag{6}$$

$$\beta = \delta + \tau \tag{7}$$

Thus, from Eqs. (1) through (7), we get

$$\frac{B_n}{F_n} = \frac{\kappa(\cos\beta + 1) - \sin\beta}{\text{DENO}} = C_b \tag{8}$$

$$\frac{B_n}{F_n} = \frac{\mu_k(\cos\alpha - 1) + \sin\alpha}{\text{DENO}} = C_r \tag{9}$$

where

$$\begin{aligned}\text{DENO} = &\sin(\alpha+\beta) + \mu_k[\cos(\alpha+\beta) - \cos\beta] \\ &- \kappa[\cos(\alpha+\beta) + \cos\alpha] \\ &+ \mu_k\kappa[\sin(\alpha+\beta) + \sin\alpha - \sin\beta]\end{aligned}$$

under the assumption that $G_w \ll F_n$.

Therefore, F_t, B_n, B_t, R_n, and R_t can be expressed as:

$$F_t = (\mu_k C_b + \kappa C_r) F_n \tag{10}$$

$$B_n = C_b F_n \tag{11}$$

$$B_t = \mu_k C_b F_n \tag{12}$$

$$R_n = C_r F_n \tag{13}$$

$$R_t = \kappa C_r F_n \tag{14}$$

Figure 3 shows the changes of these forces according to the change of κ. μ_k, μ_r, α, and β were taken as 0.3, 0.4, 57.8°, and 6°, respectively. When the workpiece is a plain carbon steel, the friction coefficient between the workpiece and the grinding wheel, μ_s, is 0.4 (Malkin, 1989), and κ corresponding to this value is 0.22 (Fig. 3). Thus, it can be assumed that the lower bound of κ is 0.22 and the upper bound of κ is 0.4 from Eq. (5).

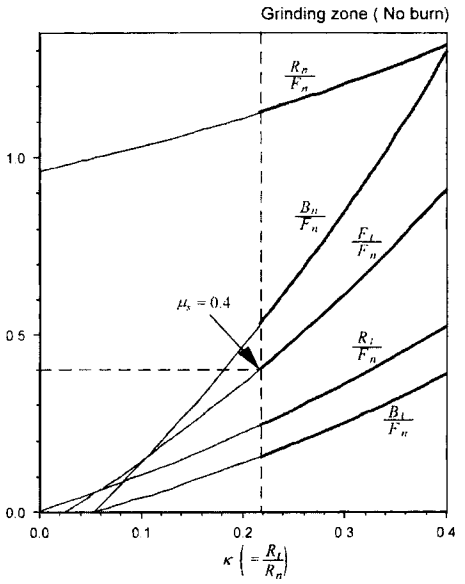

Fig. 3 The changes of forces according to the change of κ (Workpiece material : steel, μ_k=0.3, α= 57.8°, β=6°)

Figure 4 shows the cross-sectional diagram of the elastic compression at the contact point of cylindrical bodies. When the contact widths at the contact points are much smaller than the radii of these bodies, half of contact width, a, and the deflection of the upper half center body at the contact point, δ_m, are given as:

$$a = \sqrt{\frac{4PR^*}{\pi E^*}} \quad \left(\frac{1}{R^*} = \frac{1}{R} + \frac{1}{R_1},\ \frac{1}{E^*} = \frac{1-\nu^2}{E} + \frac{1-\nu_1^2}{E_1}\right) \tag{15}$$

$$\delta_m = P\frac{(1-\nu^2)}{\pi E}\{2\ln(4R/a) - 1\} \tag{16}$$

where P is the compressive load per unit axial length, R is the radius of central body, and E, E_1, ν and ν_1 are the moduli of elasticity and the Poisson's ratios of each body, respectively (Johnson, 1987).

During the centerless grinding process, the external forces on the workpiece satisfy equilibrium conditions. The normal force applied at the regulating wheel contact point can be given as a function of F_n, as shown in Eq. (13). Hence, half of the contact width, a_r, at the regulating wheel

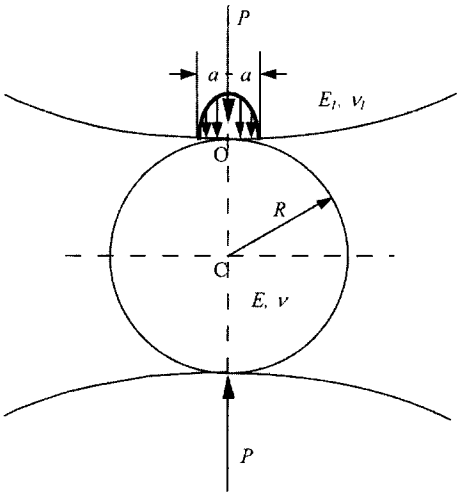

Fig. 4 Cross-sectional diagram of the elastic compression at contact point of cylindrical bodies (Johnson, 1987)

contact point deflection of the workpiece, δ_{wr}, due to R_n and the deflection of the regulating wheel, δ_r, can be expressed as

$$a_r=\sqrt{\frac{4C_rF_nR_r^*}{\pi E_r^*}} \quad \left(\frac{1}{R_r^*}=\frac{1}{R}+\frac{1}{R_r},\ \frac{1}{E_r^*}=\frac{1-\nu^2}{E}+\frac{1-\nu_r^2}{E_r}\right) \tag{17}$$

$$\delta_{wr}=C_r\frac{(1-\nu^2)}{\pi E}\{2\ln(4R/a_r)-1\}F_n \tag{18}$$

$$\delta_r=C_r\frac{(1-\nu_r^2)}{\pi E_r}\{2\ln(4R_r/a_r)-1\}F_n \tag{19}$$

where R_r is the radius of the regulating wheel, E_r is the modulus of elasticity of the regulating wheel, and ν_r is the Poisson's ratio of the regulating wheel. Similarly, the normal force applied at the work-rest blade contact point can be found in Eq. (11), and half of the contact width, a_b, at the work-rest blade contact point and deflection of the workpiece, δ_{wb}, due to B_n can be expressed as

$$a_b=\sqrt{\frac{4C_bF_nR_b^*}{\pi E_b^*}} \quad \left(\frac{1}{R_b^*}=\frac{1}{R}+\frac{1}{\infty}=\frac{1}{R},\ \frac{1}{E_b^*}=\frac{1-\nu^2}{E}+\frac{1-\nu_b^2}{E_b}\right) \tag{20}$$

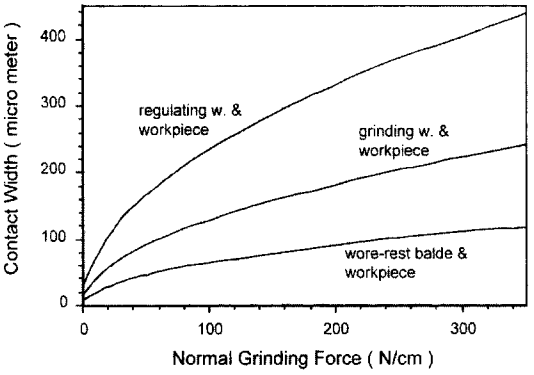

Fig. 5 Contact width at each contact point

$$\delta_{wb}=C_b\frac{(1-\nu^2)}{\pi E}\{2\ln(4R/a_b)-1\}F_n \tag{21}$$

where E_b is the modulus of elasticity of the regulating wheel and ν_b is the Poisson's ratio of the regulating wheel. The work-rest blade was assumed as a simple column, and the deflection of the work-rest blade, δ_b, is given as:

$$\delta_b=\frac{C_b}{E_b}\frac{h}{t}F_n \tag{22}$$

where h is the height of the work-rest blade and t is the thickness.

The contact width and deflection at each contact point are calculated as functions of F_n using Eqs. (17) through (22) under the following conditions: $\alpha=57.8°$, $\beta=6°$, $R=15$ mm, $R_g=271$ mm, $R_r=151$ mm, and using steel ($E=20.7$ MN/cm^2, $\nu=0.3$) as the workpiece material. κ was assumed to be 0.31, the medium value in the grinding zone in shown Fig. 3. Mechanical properties of the regulating wheel, E_r and ν_r, were assumed as 1.55 MN/cm^2 and 0.25, respectively (Kingery et al., 1976). The work-rest blade material was assumed to be tungsten carbide, and the mechanical properties, E_b and ν_b, and the dimensions, h and t, were assumed as 55.1 MN/cm^2, 0.3, 60 mm, and 7 mm, respectively. The resultant contact width and deflection are shown in Figs. 5 through 7.

Figure 5 shows that the contact width at the regulating wheel contact point is wider than that at the work-rest blade contact point. Since the wheels and workpiece are cylindrical bodies, it

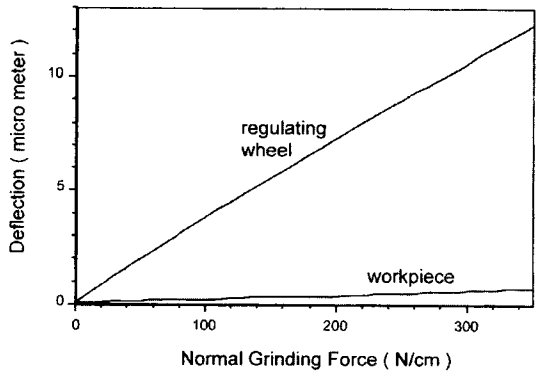

Fig. 6 Deflections at regulating wheel contact point

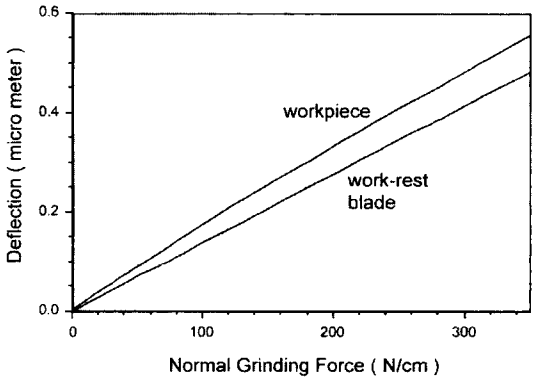

Fig. 7 Deflections at work-rest blade contact point

can be assumed that the local deflection of the regulating wheel at the workpiece contact point will be greater than that of the work-rest blade.

Normally, the theoretical contact stiffness is larger than the measured one, and theoretically the calculated contact area is always smaller than the measured one (Snoeys and Wang, 1968). Thus, it can be expected that the contact width and the deflection of elements at each contact point during an actual centerless grinding process will be larger than the values that are calculated in this section.

3. Least Squares Contact Line

Through the force and deflection analyses in the previous section, it can be deduced that the workpiece is engaged with the wheels over some contact area. Normally, the surface of a cylindrical part shows not only the circumferential

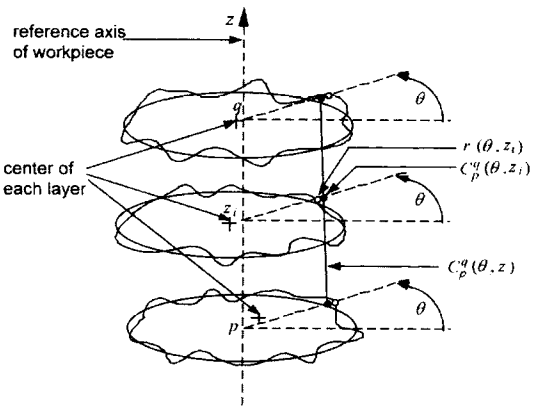

Fig. 8 Contact line fitted by least squares (LSCL)

waviness but also an axial waviness. Like the circumferential waviness, the axial waviness also has peaks and valleys. To generate the contact line, the peaks are assumed to deflect elastically and engage with the wheel surface, and some valleys are not in contact with the wheel. Therefore, the contact line was assumed as a line passing through the middle of peaks and valleys. Among the lines that satisfy this assumption, a straight line fitted by least squares was selected as the contact line because of mathematical simplicity. Fig. 8 shows the difference between the surface points of the workpiece and the points calculated from the contact line fitted by least squares, $C_p^q(\theta, z)$. The mathematical form of the least squares contact line (LSCL) is as follows:

$$C_p^q(\theta, z) = A + Bz \quad (p \le z \le q) \tag{23}$$

$$A = \{\Sigma r(\theta, z_i)\}/n - B\{\Sigma z_i\}/n \tag{24}$$

$$B = \frac{\Sigma\{z_i r(\theta, z_i)\} - [\{\Sigma z_i\}\{\Sigma r(\theta, z_i)\}/n]}{\Sigma z_i^2 - \{\Sigma z_i\}^2/n} \quad \left(p \le z_i \le q,\ n = \frac{q-p}{\Delta z}\right) \tag{25}$$

where $r(\theta, z_i)$ is the distance from any reference point in the cross-section of the workpiece at axial distance z_i from the leading end to the periphery of the workpiece at angle θ from the reference line, z is the axial distance from the leading end of the workpiece to the simulation layer, p is a lower bound for LSCL, q is an upper bound for LSCL, and n is the number of layers

between p and q.

During an infeed grinding process, the full width of the workpiece contacts the wheels. So the lower bound and the upper bound of z for LSCL are 0 and w, respectively. Also, there are interference phenomena in a centerless grinding process (Kim et al., 1992b). Thus, if the angular displacement difference between the real regulating wheel contact point at rotation θ and its ideal contact point, $r(\theta-\pi+\beta, z_i)$, is ξ_{θ,z_i}, the LSCL equation for the regulating wheel contact line, $C_o^w(\theta-\pi+\beta, z)$, is as follows:

$$C_o^w(\theta-\pi+\beta, z)=A_r+B_rz \quad (0\le z\le w) \tag{26}$$

$$A_r=[\sum\{\cos(\xi_{\theta,z_i})\, r(\theta-\pi+\beta+\xi_{\theta,z_i}, z_i)\}]/n-B_r\{\sum z_i\}/n \tag{27}$$

$$B_r=\frac{\sum[z_i\{\cos(\xi_{\theta,z_i})\, r(\theta-\pi+\beta+\xi_{\theta,z_i}, z_i)\}]-[\{\sum z_i\}\{\sum(\cos(\xi_{\theta,z_i})\, r(\theta-\pi+\beta+\xi_{\theta,z_i}, z_i))\}/n]}{\sum z_i^2-\{\sum z_i\}^2/n} \tag{28}$$
$$\left(0\le z_i\le w,\ n=\frac{w}{\Delta z}\right)$$

where n is the number of measurement layers of the workpiece.

Similarly, if the angular displacement difference between the real work-rest blade contact point and its ideal contact point, $r(\theta-\alpha, z_i)$, is $\zeta_{\theta,zi}$, LSCL equation for the work-rest blade contact line, $C_0^w(\theta-\alpha, z)$, can be expressed as follows:

$$C_o^w(\theta-\alpha, z)=A_b+B_bz \quad (0\le z\le w) \tag{29}$$

$$A_b=[\sum\{\cos(\zeta_{\theta,z_i})\, r(\theta-\alpha+\zeta_{\theta,z_i}, z_i)\}]/n-B_b\{\sum z_i\}/n \tag{30}$$

$$B_b=\frac{\sum[z_i\{\cos(\zeta_{\theta,z_i})\, r(\theta-\alpha+\zeta_{\theta,z_i}, z_i)\}]-[\{\sum z_i\}\{\sum(\cos(\zeta_{\theta,z_i})\, r(\theta-\alpha+\zeta_{\theta,z_i}, z_i))\}/n]}{\sum z_i^2-\{\sum z_i\}^2/n} \tag{31}$$
$$\left(0\le z_i\le w,\ n=\frac{w}{\Delta z}\right)$$

4. Three Dimensional Model

When the irregularities of the workpiece occur either at the work-rest blade or at the regulating wheel, the workpiece will be displaced and the apparent depth of cut at the grinding wheel contact point will be changed. Thus, the apparent depth of cut, $D(\theta, \eta, z)$, is given as

$$\begin{aligned} D(\theta, \eta, z)=&D(0, 0, z)+\cos\delta\{X(\theta)-X(0)\}\\ &-\frac{\sin\beta}{\sin(\alpha+\beta)}\{C_0^w(\theta-\alpha, z)-C_0^w(-\alpha, z)\}\\ &+\frac{\sin\alpha}{\sin(\alpha+\beta)}\{C_0^w\{\theta-\pi+\beta, z)-C_0^w\{-\pi+\beta, z)\}\\ &+\{\cos(\eta)\, r(\theta+\eta, z)-r(-2\pi, z)\} \end{aligned} \tag{32}$$

where $X(\theta)$ is the magnitude of the infeed motion at θ, δ is the angle between infeed motion and grinding wheel contact normal, and η is the angular displacement difference between the real grinding wheel contact point and the ideal contact point.

The machining factor, K_m, and threshold grinding force, P_0, are available for the full length of the workpiece. To apply these values to this model, these values must be divided by the number of layers, n. Likewise, if the elasticity factor, K_e, is assumed as a parallel connection of n springs, this factor can be regarded as K_e/n. Therefore, if $\eta_{\max}$ is the angular displacement difference between the point which has the maximum apparent depth of cut, $D(\theta, \eta_{\max}, z_i)$, and the ideal contact point, $r(\theta, z_i)$ of layer i, the deflection of the system, $x(\theta, z_i)$, is given as:

$$\begin{aligned} x(\theta, z_i)=&\frac{f_n(\theta, z_i)}{(K_e/n)}\\ =&\cos(\eta_{\max})\{D(\theta, \eta_{\max}, z_i)-L(\theta, \eta_{\max}, z_i)\} \end{aligned} \tag{33}$$

where $f_n(\theta, z_i)$ is the normal grinding force acting at layer i, and $L(\theta, \eta_{\max}, z_i)$ is the true depth of cut at the point which has the maximum apparent depth of cut.

If $r(\theta+\eta_k, z_i)$ is one of the grinding wheel contact points of this layer, the true depth of cut, $L(\theta, \eta_\kappa, z_i)$, with its corresponding $D(\theta, \eta_k, z_i)$ is given as:

$$\begin{aligned} L(\theta, \eta_k, z_i)=&\frac{\cos(\eta_k)\, D(\theta, \eta_k, z_i)-x(\theta, z_i)}{\cos(\eta_k)}\\ &(\text{when } \cos(\eta_k)\, D(\theta, \eta_k, z_i)\ge x(\theta, z_i)) \end{aligned} \tag{34}$$

When $\cos(\eta_k)\, D(\theta, \kappa_k, z_i)$ is less than the deflection of the system, $x(\theta, z_i)$, material removal will be zero. Thus $f_n(\theta, z_i)$ can be formulated as a function of the true depth of cut:

$$f_n(\theta, z_i)=\frac{K_m}{n}\left[\sum_{for\ all\ k} L(\theta, \eta_k, z_i)\right]+\frac{P_0}{n} \tag{35}$$

If there are positive $x(\theta, z_i)$ and $L(\theta, \eta_k, z_i)$, which satisfy Eqs. (33), (34), and (35) simultaneously, actual material removal can happen. Therefore, if a peripheral point, $r_{old}(\theta+\eta_k, z_i)$, is ground at rotation θ, then this peripheral point, $r_{new}(\theta+\eta_k, z_i)$, just after this instantaneous grinding can be expressed as

$$r_{new}(\theta+\eta_k, z_i)=r_{old}(\theta+\eta_k, z_i)-L(\theta, \eta_k, z_i) \quad (36)$$

5. Experiment and Simulation

The pre-grinding shape of the specimens in this experiment was a partially flat cylindrical hollow bar as shown in Fig. 9. This shape is easy to control and includes all orders of harmonics below the fortieth with the largest amplitudes obtained for the lowest orders (Rowe et al., 1965). It is useful to find any effect of the grinding variables on a certain order of waviness. Three types of workpieces were used in this work. The first type of specimen had a flat along its axis. The second and third types had flats whose lengths were 2/3 and 1/3 of the specimen length, respectively. The material of the specimens was a hardened steel with Rockwell C hardness of 62-63. The roundness error, straightness, and taper of the pre-grinding specimens, except the flat area, were

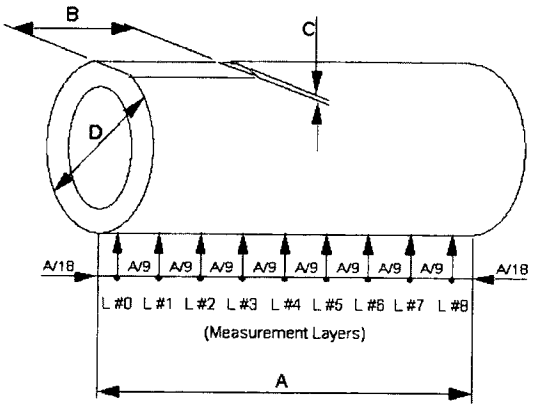

(unit: mm)

	Type	A (±0.3)	B	C (±0.004)	D (±0.002)
Infeed	I1	75	75 ±0.3	0.05	24.990
	I2		50 ±0.5		
	I3		25 ±0.5		

Fig. 9 Details of the specimen geometry

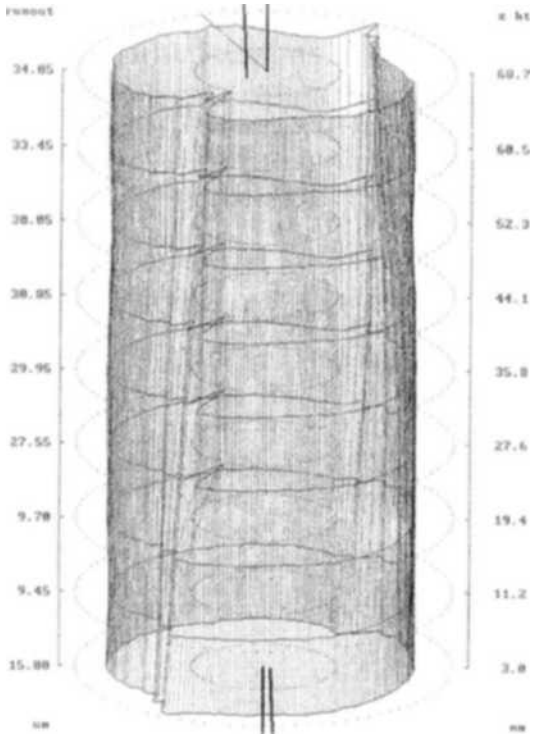

Fig. 10 Experimental result (specimen type: I2, β=4°)

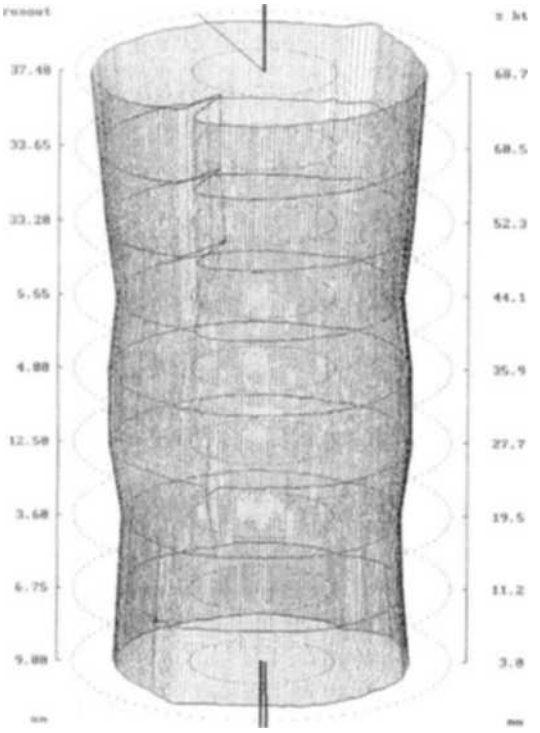

Fig. 11 Experimental result (specimen type: I3, β=4°)

within 2 μm, and the deviation of the flat depth was within 4 μm. The grinding machine and conditions are given in Table 1.

To investigate the ground specimens 3-dimensionally, nine measuring layers (from 0 to 8) of each specimen were selected and their locations are shown in Fig. 9. The cylindricity profiles were measured on the Talyrond 252 machine from Rank Taylor Hobson Co. The measured cylindricity profiles are presented in Figs. 10 and 11.

To figure out the geometry of a ground workpiece, computer simulation techniques are applied to the analytical models. In this simulation model, a cylindrical coordinate system is used. The z-axis of this coordinate system is parallel to the geometric axis of the pre-grinding workpiece. The origin of the z-axis is fixed at an arbitrary position around the geometric center of the pre-grinding 2-D profile of the workpiece leading end. To generate a 3-D geometric shape of the workpiece, it is segmented into 9 equi-spaced layers, and the periphery of each layer is divided by 360 equal angles. The distance, which is measured from the axis of a layer to the angularly equi-spaced periphery point of this layer, reflects the instantaneous radius of this surface, $r(\theta, z)$. All layers are then rotated incrementally in 360 steps per revolution. Each time, the new workpiece position is found and the regulating wheel contact line and the work-rest blade contact line are generated using the least squares contact line model from the real contact points of each layer. Then, the apparent depth of cut values, D, at the feasible grinding contact points are calculated using the contact lines for each layer. The next step is similar to the 2-D simulation (Kim et al., 1992).

Simulation was carried out under the same conditions as shown in Table 1. The threshold grinding force, P_0, of 210 N was quoted from the reference (ASM International, 1989), and the machining factor, K_m, was calculated as 195.5 MN/m (Kim et al., 1992). The elasticity factor, K_e, of 20 MN/m was cited from the reference

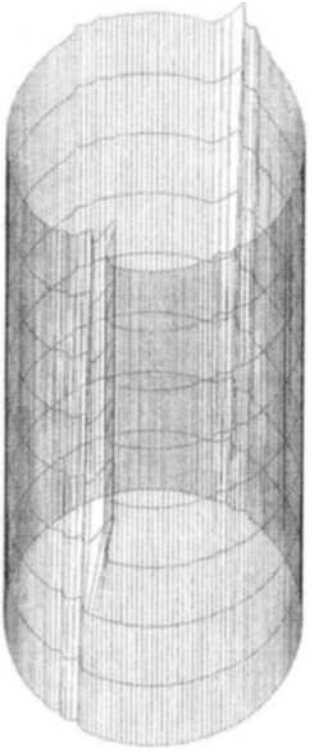

Fig. 12 Simulation result (specimen type: I2, β=4°)

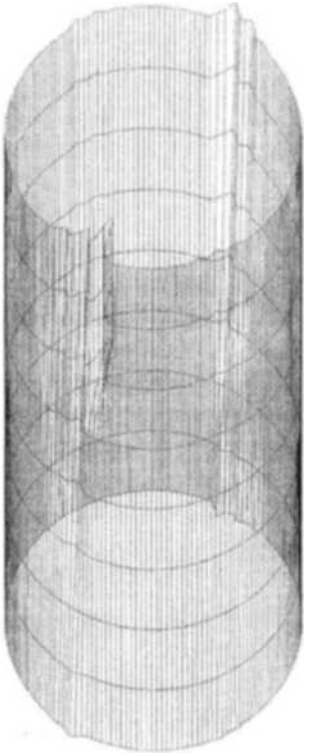

Fig. 13 Simulation result (specimen type: I3, β=4°)

(Reshetov and Portman, 1988). Simulation results are shown in Figs. 12-13.

6. Results and Discussion

The simulation results in Figs. 12-13 show that the number of lobes and the angular displacement of the peaks and the corresponding valleys are similar to the corresponding experimental results shown in Figs. 10-11. For the specimen type I2, Figure 12 shows the gradually decreasing trend of the waviness amplitude toward the round end, while maintaining the characteristics of the roundness profile (number of lobes and locations of the major peaks and valleys). Figure 13 shows the simulation result of type I3 specimen. As in the case of type I2 specimen, the amplitude of waviness gradually decreases, and it becomes almost 0 at layer #6. The roundness profile of the round end (layer #8) shows 180° phase shift of all peaks and valleys. The corresponding experimental results (Fig. 11) show similar characteristics. It can be seen in type I2 specimen that the specimen wobbles around the round end (layer #8). For type I3 specimen, it wobbles around the mid-section (near layer #6). For centerless infeed grinding, workpiece reorientation is shown to greatly influence the cylindricity of the ground workpiece.

As expected, it can be seen that the contact points which are not in the same analyzed layer have an effect on the roundness mechanism of this layer. This means that the centerless infeed grinding process must be understood 3-dimensionally, even though the 2-D rounding mechanism provides adequate guidelines for machine set-up. Both experimental and simulation results reveal that the shape of ground part is affected not only by the circumferential waviness but also by the axial waviness of the initial shape.

7. Conclusion

The objective of this research is to develop a computer simulation method to investigate the mechanism of cylindrical form generation in the centerless infeed grinding process. The 3-D infeed model was developed based on the 2-D infeed model and the concept of least squares contact line (LSCL). LSCLs were formulated to include the effects of contact points which are not on a straight line, and the interference phenomena. To validate the feasibility of LSCL modeling, force and deflection at a contact point were analyzed.

All the simulation results show that the number of lobes and the angular displacement of peaks and corresponding valleys are similar to the corresponding experimental results. Also, it was found that the workpiece reorientation plays an important role in the cylindricity of the ground part.

References

ASM International, 1989, *Metals Handbook, 9th Edition, Vol. 16 Machining*, pp. 422, 448.

Dall, A. H., 1946, "Rounding Effect in Centerless Grinding," *Mechanical Engineering*, Vol. 68, No. 4, ASME, pp. 325~329.

Johnson, K. L., 1987, *Contact Mechanics*, Cambridge University Press, pp. 84~134.

Kim, K., Chu, C. N. and Barash, M. M., 1992a, "Roundness Generation during Centerless Infeed Grinding," *Transactions of NAMRI of SME*, 20, pp. 167~172.

Kim, K., Chu, C. N. and Barash, M. M., 1992b, *Cylindricity Control in Precision Centerless Grinding*, Technical Report TR-ERC 92-6, Purdue University, pp. 23~31, 77~86.

Kingery, W. D., Bowen, H. K. and Uhlmann, D. R., 1976, *Introduction to Ceramics 2nd ed.*, John Wiley & Sons, pp. 768~783.

Malkin, S., 1989, Grinding Technology, Ellis Horwood Limited, pp. 116.

Reshetov, D. N. and Portman, V. T, 1988, *Accuracy of Machine Tools*, ASME Press, p. 275.

Rowe, W. B. and Barash, M. M., 1964, "Computer Method for Investigating the Inherent Accuracy of Centerless Grinding," *Int. J. Mach. Tool Des. Res.*, Vol. 4, pp. 91~116.

Rowe, W. B., Barash, M. M. and Koenigsberger, F., 1965, "Some Roundness Characteristics of Centerless Grinding," *Int. J. Mach. Tool Des. Res.*, Vol. 5, pp. 203~215.

Snoeys, R., and Wang, I-C., 1968, "Analysis of the Static and Dynamic Stiffnesses of the Grinding Wheel Surface," *Proc. 9th Int'l Mach. Tool Des. and Res. Conf. Part 2*, pp. 1133~1148.

Yonetsu, S., 1959, "Forming Mechanism of Cylindrical Work in Centerless Grinding," *Proc. Fujihara Memorial Faculty of Engineering*, Keio Univ., Vol. 12, No. 47, pp. 27~45.